Stability and transient effects in nanosecond ultraviolet light filaments in air

Thomas A. Niday* and Ewan M. Wright†
Optical Sciences Center, University of Arizona, Tucson, Arizona 85721, USA

Miroslav Kolesik‡ and Jerry V. Moloney§
Arizona Center for Mathematical Sciences, University of Arizona, Tucson, Arizona 85721, USA
(Received 13 August 2004; revised manuscript received 10 May 2005; published 19 July 2005)

We investigate the transient behavior and stability of nanosecond duration ultraviolet pulses propagating in air. Both the transient behavior arising from the finite pulse duration and the modulational instability, are found to cause pulses to fragment over lengths on the scale of meters. We discuss the theoretical and experimental implications of the instability and transient effects for long duration pulse propagating in air and generating filaments. In particular, our results imply that continuous-wave models are very limited when used to predict dynamical properties of pulse propagation.

DOI: 10.1103/PhysRevE.72.016618 PACS number(s): 42.65.Tg, 42.65.Jx, 42.65.Sf, 52.38.Hb

I. INTRODUCTION

Ultrashort high-intensity laser pulses in the form of light filaments can propagate for long distances in air by inducing nonlinear optical effects. By long distance, we mean distances larger than the Rayleigh range calculated from the filament transverse width. The primary nonlinear effect is self-focusing, caused by the intensity-dependent refractive index induced by the optical Kerr effect [1]. If the peak power exceeds a certain critical power, self-focusing overcomes diffraction, focusing the beam tighter, and in turn intensifying the nonlinear effects. At some point, the field becomes strong enough to ionize the molecules in the air, and higher-order nonlinear effects such as multiphoton absorption, plasma absorption, and plasma defocusing stop the collapse [2,3]. The propagation depends on the interaction between self-focusing and the various collapse arrest mechanisms. A dynamic balance between these effects results in self-guiding of the pulse through the generation of filaments [3–5].

Tightly focused light filaments have the potential to pass through atmospheric turbulence and scattering media such as clouds [6] with less distortion than continuous-wave (CW) beam encounters. As an ultrashort pulse compresses temporally, it can generate a broad spectrum [7–9]. This might be used in future light detection and ranging (LIDAR) remote sensing techniques for spectral analysis of pollutants or hazardous compounds in the atmosphere [10,11]. The plasma channels generated by light filaments may also have the ability to enable laser induced lightning [12,13]. Experiments have been done with atmospheric propagation of ultrashort pulses [6,9,11,14]. Propagation distances as long as 12 km vertical in the atmosphere (claimed through detection of backscattered supercontinuum generation) [10,14] and hundreds of meters [15] up to 2 km horizontal in air [16] have been investigated.

Much of the theoretical and experimental work on filaments has been conducted in the infrared (IR), typically with wavelengths near 800 nm and pulse durations on the order of hundreds of fs [6,9,15,17–24]; in some cases the pulses are prepared longer with initial chirp [8,10,11,14] to compensate for group velocity dispersion (GVD). However, some researchers have begun investigating the possibility of creating self-guided pulses in the ultraviolet (UV) wavelength region, near 248 nm. UV filaments have been studied and contrasted with those in the IR [2]. For example, Schwarz *et al.* [25,26] have performed experiments using a frequency tripled Ti:sapphire laser to obtain filaments at 248 nm. They created pulse durations between 600 fs and several ps, and observed filaments that propagated for 12 m. Tzortzakis *et al.* performed experiments for both 450 fs and 5 ps pulses, and observed UV filaments at 248 nm that propagate stably for 4 m [4].

It has recently been proposed that the results for UV filaments should scale with respect to increasing the pulse duration [25–27], resulting in long distance propagation of long duration pulses, with higher total energy. This was suggested because it was observed that the balance of self-focusing and plasma defocusing for UV filaments appears to depend only on the intensity of the field [25]. Additionally, the reduced contribution from avalanche ionization in the UV extends the upper limit on the pulse duration up to tens of nanoseconds, four orders of magnitude larger than in the infrared [27]. This has been investigated by Schwarz and Diels, who have developed a semianalytical solution for long pulses in the UV [27], based on an effective instantaneous plasma response. Other authors, for shorter pulses, have employed the same approach by examining the integrated contribution of the plasma at an arbitrary central time slice of the pulse [15,28,29]. However, we will see that the problem of temporal stability is critically important, and may be overlooked by using such approximations. To investigate this question of stability, we here use a linear perturbation analysis and a

*Present address: Air Force Institute of Technology, Wright-Patterson AFB, Ohio, 45433; Electronic address: thomas.niday@afit.edu
†Electronic address: ewan.wright@optics.arizona.edu
‡Electronic address: kolesik@acms.arizona.edu
§Electronic address: jml@acms.arizona.edu

three-dimensional numerical simulation. The results indicate that long UV pulses suffer from a strong instability, and that the time-independent model is inadequate to describe them.

In the remainder of this paper, we first review the time-independent model used by Schwarz and Diels [27] in Sec. II. In Sec. III, we discuss the stability of steady state solutions to the time-independent model. Section IV gives numerical evidence of the growth of the unstable modes identified in the stability analysis, and Sec. V describes the 3D simulation of a pulse which exhibits the instability. Then, in Sec. VI, we discuss the implications of our results to UV pulse propagation as well as theoretical approaches that use time-independent models.

II. TIME-INDEPENDENT MODEL

A. Propagation equation

In this section, we review and extend the method of Schwarz and Diels [27], to provide a foundation for our investigation. We start with the following equation for propagation [25] of the electric field envelope $\mathcal{E}(x,y,z,t)$:

$$\frac{\partial \mathcal{E}}{\partial z} = \frac{i}{2k}\nabla_\perp^2 \mathcal{E} + ik_0 n_2 |\mathcal{E}|^2 \mathcal{E} - \frac{\beta^{(K)}}{2}|\mathcal{E}|^{2K-2}\mathcal{E} - \frac{\sigma}{2}(1+i\omega\tau)\rho\mathcal{E}, \tag{1}$$

where the z axis is the direction of propagation. Here $|\mathcal{E}|^2$ is the field intensity, k is the wave number, k_0 is the wave number in free space, n_2 is the self-focusing index in m^2/W, $\beta^{(K)}$ is the MPI coeffcient for order K, σ is the cross section for inverse bremsstrahlung, ω is the optical frequency, and τ is the characteristic electron collision time [25]. The electron density ρ of the plasma is described by

$$\frac{\partial \rho}{\partial t} = \frac{\beta^{(K)}|\mathcal{E}|^{2K}}{K\hbar\omega} - \alpha\rho^2 \equiv b|\mathcal{E}|^{2K} - \alpha\rho^2, \tag{2}$$

where α is an electron-positive ion recombination coefficient [27]. Following Ref. [27], we assume that the pulse durations are short enough to neglect avalanche ionization. In steady state, the left-hand side of Eq. (2) is zero, and ρ is a simple function of the field intensity.

In the model used by Schwarz and Diels, the steady state ansatz allows one to express the plasma density ρ as a power of the field strength or intensity. This is only true for certain pulse durations [27]. First, if the pulses are short enough, less than tens of nanoseconds, avalanche ionization can be neglected. If the pulses are long enough so that the plasma has time to reach steady state, they set $\partial\rho/\partial t = 0$. This rise time is on the order of 30–200 ps, depending on the model parameters [26,27].

In steady state, $\rho = \sqrt{b/\alpha}|\mathcal{E}|^K$, where $b \equiv \beta^{(K)}/K\hbar\omega$. Thus the plasma response term can be replaced by an effective $n_K|\mathcal{E}|^K\mathcal{E}$ nonlinear index term. For UV pulses at 248 nm, $K=3$, and $\rho \propto |\mathcal{E}|^3$, so Schwarz and Diels replace the plasma term by an effective n_3 term. They derive the value of this term as

TABLE I. Parameters used in propagation.

Parameter	Name	Value	Units
Background index	n_0	1	
Self-focusing index	n_2	7.8×10^{-23}	m^2/W
Plasma nonlinear index	n_3	-3.3×10^{-31}	$m^3/W^{3/2}$
MPI order	K	3	
Wavelength	λ	248	nm
MPI coefficient	$\beta^{(3)}$	3.9×10^{-34}	m^3/W^2
Recombination loss	α	1.1×10^{-12}	m^3/s
Inverse bremsstrahlung cross section	σ	5.2×10^{-25}	m^2
Electron collision time	τ	3.5×10^{-13}	s
Density of oxygen	N_0	5.4×10^{24}	m^{-3}
Three-photon absorption cross section	$\sigma^{(3)}$	3×10^{-41}	m^6s^2/J^3
Linear absorption loss	α_L	2.5×10^{-4}	m^{-1}
X grid spacing	Δx	8.0	μm
Time step	Δt	1.0×10^{-12}	s
Z propagation step	Δz	0.5	mm

$$n_3 = -\sqrt{\frac{\sigma^{(3)}N_0}{\alpha}}\frac{e^2}{2n_0\omega^2 m_e \epsilon_0}, \tag{3}$$

where $\sigma^{(3)}$ is a three-photon absorption cross section, N_0 is the density of oxygen molecules, and e and m_e are the charge and mass of the electron, using a model for the electron plasma [27]. If losses are neglected, Eq. (1) reduces to

$$\frac{\partial \mathcal{E}}{\partial z} = \frac{i}{2k}\nabla_\perp^2 \mathcal{E} + ik_0 n_2 |\mathcal{E}|^2 \mathcal{E} + ik_0 n_3 |\mathcal{E}|^3 \mathcal{E}. \tag{4}$$

Note that the plasma defocusing coefficient $\sigma\omega\tau\rho/2$ from Eq. (1) is equal to $k_0 n_3 |\mathcal{E}|^3$, given the steady state dependence of ρ on $|\mathcal{E}|^3$, for the parameters in Table I.

B. Aberrationless modification

In Schwarz and Diels [27], the electric field amplitude $\mathcal{E}(r,z)$ for a cylindrically symmetric field is assumed to be a Gaussian with $r^2 = x^2 + y^2$. To proceed they make the following parabolic "aberrationless" approximation for powers of the electric field [27]:

$$|\mathcal{E}(z,r)|^a = \left(\frac{w_0}{w}\mathcal{E}_0 e^{-r^2/w^2}\right)^a \approx \left(\frac{w_0}{w}\mathcal{E}_0\right)^a \left(1 - a\frac{r^2}{w^2}\right). \quad (5)$$

This is substituted into the $|\mathcal{E}|^2$ and $|\mathcal{E}|^3$ terms in the nonlinear polarization, and terms are matched based on their order in r^2/w^2. One consequence of this Taylor series approximation is that the critical power obtained using their analysis is one-fourth the critical power that is normally obtained in theories of self-focusing [30–32]. This factor of four comes from the the use of the Taylor series approximation instead of a modified power series based on a moments method or variational method [33–35].

We make such a modified aberrationless approximation, based on minimizing the mean square error in the polynomial approximation of the exponential [35,36]. With such a method, the aberrationless approximation for $|\mathcal{E}|^2$ becomes [35]

$$e^{-2r^2/w^2} \approx \left(\frac{3}{4} - \frac{1}{2}\frac{r^2}{w^2}\right). \quad (6)$$

This approximation will change the critical power to the accepted value. For the plasma term, which depends on $|\mathcal{E}|^3$, the approximation becomes

$$e^{-3r^2/w^2} \approx \left(\frac{16}{25} - \frac{12}{25}\frac{r^2}{w^2}\right). \quad (7)$$

With these improved approximations, the equation for the evolution of the beam width w is given by Eq. (38) of Ref. [27], modified as follows:

$$\frac{\partial^2 w}{\partial z^2} = -\frac{4}{k^2}\left(\frac{P}{P_{cr}} - 1\right)\frac{1}{w^3} - \frac{24}{25}\left(\frac{2P}{\pi}\right)^{3/2}\frac{n_3}{n_0}\frac{1}{w^4}. \quad (8)$$

We next present this result in the form of a potential for an effective particle moving in one dimension whose coordinate w represents the beam width. The potential well model for nonlinear beam propagation is often used and is a direct consequence of using a variational technique [31,33,37–39]. Using the above, we can write $(dw/dz)^2 = 2[E - U(w)]$, where

$$U(w) = -\frac{2}{k^2}\left(\frac{P}{P_{cr}} - 1\right)\frac{1}{w^2} - \frac{8}{25}\left(\frac{2P}{\pi}\right)^{3/2}\frac{n_3}{n_0}\frac{1}{w^3} \quad (9)$$

is the effective potential, $E = U(w_0) + w_0^2/(2R_0^2)$ is the total energy, which is conserved, P is the input beam power, and P_{cr} is the critical power. The initial width w_0 of the beam gives the particle's initial location; the initial condition for the velocity is related to the radius of curvature of the beam by $dw/dz(z=0) = w_0/R_0$. The critical power obtained here as $P_{\mathrm{cr}} = \lambda_0^2/(2\pi n_0 n_2) \approx 125$ MW is four times the P_{cr} defined in Schwarz and Diels [27]. This gives a more accurate estimate of the critical power $\approx 1.86\lambda_0^2/(4\pi n_0 n_2)$ for a Gaussian beam [37,40,41].

This same equation of motion for the beam width w can be derived with an alternative approach. Wright *et al.* [31] applied the general variational result of Anderson and Bonnedal [42] to the problem of beam propagation under cubic-quintic (n_2 and n_4) nonlinearity. This variational model assumes that the beam is described by the trial function $\mathcal{E}(r,z) = \mathcal{E}_0(z)\exp[-r^2/2a^2(z) + ir^2 b(z)]$. Following their notation, we can apply the same result to the present case of a cubic-quartic nonlinearity. By considering the $n_3|\mathcal{E}|^3$ term, we find that the equation of motion for the beam width in the case of the UV filaments is

$$\frac{d^2 a}{dz^2} = \frac{1}{k^2 a^3}\left(1 - \frac{P}{P_{cr}} + \frac{24}{25}\sqrt{\frac{I_p}{I_0}}\frac{P}{P_{cr}}\frac{a_0}{a}\right). \quad (10)$$

Here a is the beam width, and a_0 the initial beam width. Note that $w = \sqrt{2}a$; converting the above to the notation of Schwarz and Diels gives a result exactly identical to Eq. (8). I_p is the peak input intensity, and I_0 is a reference intensity defined by $I_0 = (n_2/n_3)^2$. At $I = I_0$, the total nonlinear refractive index change for a plane wave is zero.

For the values in Ref. [27], $I_0 = 5.5 \times 10^{16}$ W/m^2. Following Ref. [31], we obtain a self-trapping power for a collimated Gaussian input beam

$$P_{\mathrm{ST}} = P_{\mathrm{cr}}\left(1 - \frac{24}{25}\sqrt{\frac{I_p}{I_0}}\right)^{-1}. \quad (11)$$

This self-trapping power depends on the input intensity. If $I_p > (25/24)^2 I_0$, then there will be no self-trapped solution, since power cannot be negative. For UV propagation, this predicts that there will be no self-trapped solution for $I_p > 6.0 \times 10^{16}$ W/m^2. The self-trapped power, however, can be arbitrarily large, as the beam width may increase as intensity approaches the cutoff.

C. Oscillatory solutions

Schwarz and Diels numerically integrated their evolution equation for the beam width [Eq. (38) of Ref. [27]] to predict the behavior of the quasi-steady state filaments. For comparison, we also directly solve Eq. (4), the numerical partial differential equation for propagation, using a split-step Fourier beam propagation method [43]. This illustrates the applicability of the Gaussian ansatz.

We use the numerical parameters presented in Table I, many of which are from Schwarz and Diels [27]. Additional parameters are from Ref. [25]. Some of the values in the table are not well known; the MPI coefficient is difficult to measure [44], and may vary by two orders of magnitude up or down, depending on the publication [25–27,44]. We retain the numbers from Ref. [27], for comparison to the previous work.

Figure 1 shows the potential surfaces $U(w)$ corresponding to beam powers of 100, 200, and 500 MW. The depth of the well increases with beam power. The 100 MW surface is for a power below the critical power of 125 MW, so the potential surface no longer supports a bound state. Since the binding strength of the potential depends on the power in the beam, absorption losses will cause the potential to change, and we will observe this in the oscillatory solution. The potential $U(w)$ approaches zero as $w \to \infty$. If the particle has total energy E greater than zero, it is not bound and the beam will diffract. This can be caused by the initial beam being narrower than the width corresponding to a zero of $U(w)$ (approximately 81 μm for 200 MW power), which may not be a

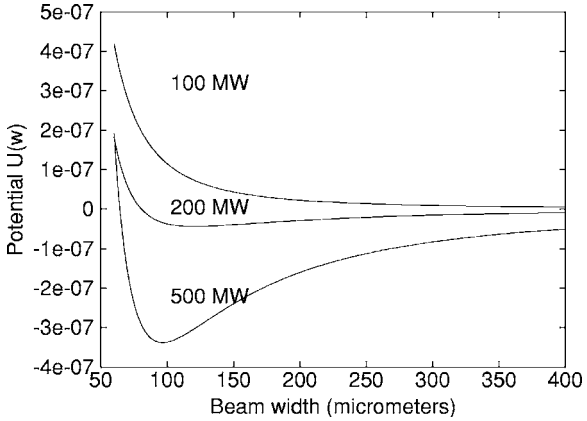

FIG. 1. Potential wells for beam powers at 100, 200, and 500 MW.

physically realistic initial condition, or the beam having too much initial curvature. For simplicity, we start at a beam waist, so $R_0=\infty$.

For our numerical simulations based on the split-step method, we characterize the beam width by its second moment. An example of our split-step simulations where the initial conditions are near the bottom of the potential well is shown in Fig. 2. Here the power was 500 MW and the initial width 100 μm, with no absorption, and small oscillations are evident. For initial conditions further displaced from the potential minimum for a 500 MW beam, such as those shown in Fig. 3, the initial conditions lead to larger oscillations in the split-step simulations, the initial width for this simulation being 200 μm. In Fig. 3 the more regular curve is the prediction from the Schwarz-Diels theory, which we see does not capture the full numerics. Figure 4 shows the evolution of a beam where the power is 200 MW and initial width is 100 μm. There are fairly consistent, larger amplitude oscillations, but again they are not constant. For starting powers larger than 1 GW, the beam quickly sheds much of its power into diffracting rings, as it adapts its form to approach an oscillatory solution, and the peak intensity is reduced. This is consistent with the existence of a maximum trapping intensity, although the observed value for this maximum trapping

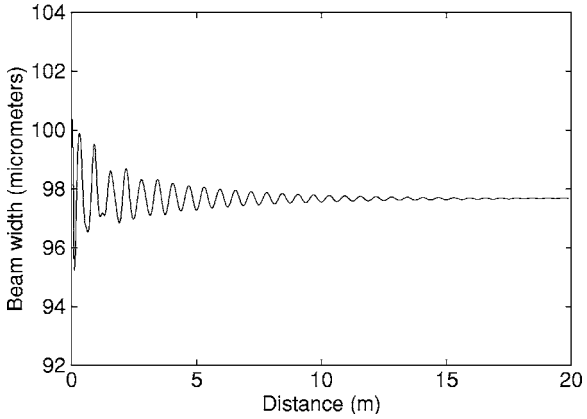

FIG. 2. Beam evolution for power of 500 MW, initial width of 100 μm, and no absorption. This set of initial conditions corresponds to a near steady state solution.

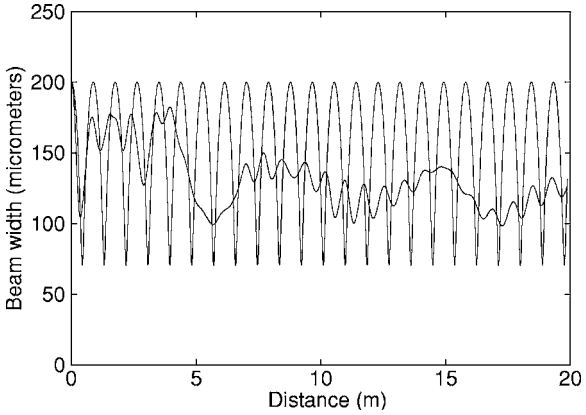

FIG. 3. Beam evolution for power of 500 MW, initial width of 200 μm, and no absorption. In this case the initial width is far from steady state, leading to nonlinear oscillations.

intensity is roughly 4×10^{16} W/m^2, instead of 6×10^{16} W/m^2 as predicted in Sec. II B. The variational approach provides an estimate for the order of magnitude of such a quantity, but cannot capture the details of features such as rings, that are beyond the starting Gaussian ansatz.

The oscillations appear to either dampen in amplitude or change chaotically for these cases. Since we have not yet included nonlinear propagation losses, the observed dampening is due to radiative losses, as the evolving solution adjusts itself by shedding power; such a system has been shown by Subbarao *et al.* to converge to an attractor [33]. If the initial condition is far from the equilibrium solution, the Gaussian beam approximation will be temporarily violated as the beam changes form. Any power that is diffracted in a ring will be absorbed by absorbing boundary conditions at the edges of the grid. The oscillatory propagation in these results is similar to that observed in studies of a medium with cubic-quintic nonlinearity [30,31,38,45].

Schwarz and Diels suggest [27] that the oscillations in beam width correspond to a steady state analog of the dynamic replenishment phenomenon [32]. However, that model explains the propagation of short pulses in air by time-dependent interactions between the leading and trailing edges of the pulse and the generated plasma; the pulse splits

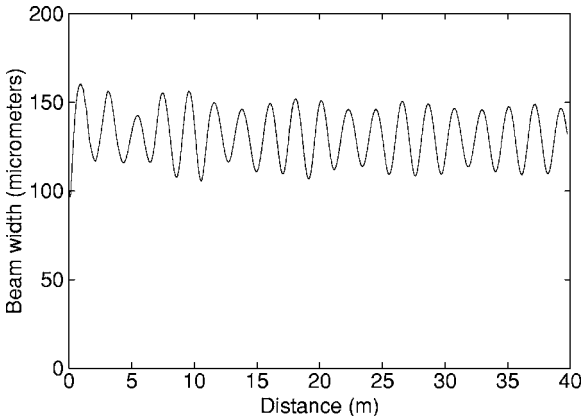

FIG. 4. Beam evolution for power of 200 MW, initial width of 100 μm, and no absorption.

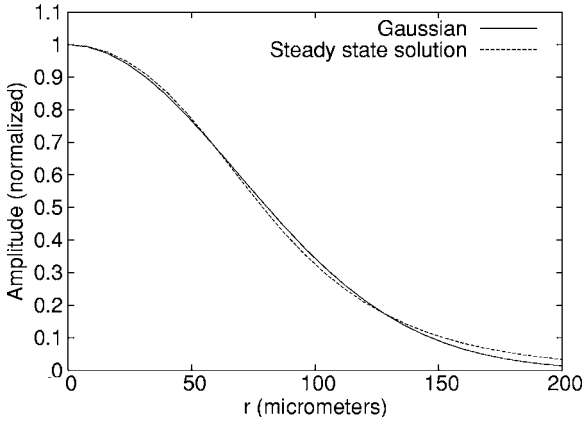

FIG. 5. Example of numerically constructed steady state solution. This solution contains a power of roughly 470 MW, and the beam width is roughly 97 μm. The peak intensity is 3.2×10^{16} W/m^2 in this example. Also shown is a Gaussian profile, with the same peak intensity and width.

in time, and power from the trailing edge replenishes the pulse. The oscillations that we consider are for a time-independent beam that can be characterized by a single width as a function of time. Additionally, any spatial pulse shaping, such as ring formation, cannot be described by the Gaussian beam ansatz.

D. Steady state solution

For the case of a 500 MW Gaussian beam that is initially 100 μm wide (Fig. 2), the width oscillations are relatively small, and the beam develops into a nearly steady state solution. We desire a steady state solution as an input for the stability analysis discussed in the following sections. To construct a steady state solution for a given peak intensity, look for a solution $\mathcal{E}(r,z)=\mathcal{E}(r)e^{i\beta z}$, with $\mathcal{E}(r)$ real, to Eq. (4). This gives

$$\nabla_\perp^2\mathcal{E}(r) = 2k\beta\mathcal{E}(r) - ik_0[n_2\mathcal{E}(r)^2 + n_3\mathcal{E}(r)^3]\mathcal{E}(r). \quad (12)$$

The nonlinear eigenvalue problem is solved, and the ground steady state beam solution for a peak intensity of 3.2×10^{16} W/m^2 is shown in Fig. 5. We chose this value for the intensity because 3.2×10^{16} W/m^2 is also the approximate peak intensity for a Gaussian beam with power 500 MW. The value of β for this solution is approximately 8.11 m^{-1}. Higher order bound states exist but exhibit azimuthal instability [46,47].

The steady state solution for this power is close to a Gaussian, but not an exact match. For pure self-focusing, the self-similar collapse solution is the Townes profile [37,40,48,49]; in that case the difference between the Gaussian and Townes profiles is important, due to the unstable nature of the solution. For the UV problem under the Schwarz-Diels model, an initial Gaussian may be nearly steady state if chosen correctly.

We ask whether such a steady state solution can represent a real pulse that maintains its shape over a long distance. Such a pulse must satisfy the duration constraints in Ref. [27]. The steady state model also assumes that the plasma responds instantaneously to changes in the electric field. It has no way to incorporate any temporal transient effects or instabilities that may arise from the finite response time of the plasma to the electric field, and this is mentioned in the analysis [27]. In the following sections, we model the stability, and simulate the propagation of long pulses to investigate these effects.

III. LINEAR STABILITY ANALYSIS

The balance between self-focusing and diffraction in the nonlinear Schrödinger equation with a strictly Kerr-type nonlinearity is unstable [1,3,37,50,51]. Only the mathematically exact solution with precisely one critical power will propagate unchanged; any deviation of the beam power from the critical power results in the beam solution collapsing or diffracting indefinitely.

More detailed models consider the spatiotemporal instability of the solutions to the nonlinear Schrödinger equation (NLSE) [52–54]. Liou *et al.* studied the spatiotemporal instability of an NLSE that only contained GVD and self-focusing terms [51]. They found that under self-focusing conditions, the interaction of spatial and temporal modulations led to an instability for either normal or anomalous GVD, which led to spatiotemporal chaos developing in the solution.

The addition of some form of saturation, such as the generation of plasma, stops filaments from collapsing indefinitely. The balance between the self-focusing collapse and saturation has been thought to explain the long life of the observed light filaments, or "bullets" that are created in beams with power equal to several critical powers [55].

However, the delayed responses of the Kerr effect and the plasma defocusing have been shown to create instabilities in short (single picosecond scale) pulses [56]. Kandidov *et al.* attributed the filamentation or breakup of short pulses to these instabilities [56].

Bian *et al.* studied the instability of plasmas generated by laser pulses [57], which they denote the ionization scattering instability. They identified a dispersion relation for the growth of unstable modes. Couairon and Bergé applied a plane wave stability analysis to the filamentation of femtosecond pulses [52]. Our linear analysis will be similar to their approach, but applied to longer time scales, rather than pulses less than a picosecond in duration.

Since many of these investigations are done for short time scales, the instabilities are identified as the breakup mechanism for a short pulse into filaments [20,37,52,56,58]. However, this raises the question of the stability of the UV long pulse solutions, which are based on an instantaneous Kerr and instantaneous plasma defocusing response. Additionally, the Schwarz-Diels model assumes that the leading edge of the pulse can develop into the steady state middle region. This requires that the steady state solution be stable, since the leading edge, which deviates from steady state, has to eventually adjust itself into a steady state solution for the model to be valid. We will first use a linear perturbation model to investigate the question of stability.

We abandon the approximation that the plasma density depends only on a power of the electric field, and return to

using a time dependent evolution equation for the plasma. Consider the evolution equation for the field, Eq. (1), and the plasma, Eq. (2). Neglecting loss terms in Eq. (1), assume that a steady state solution can be found with $\mathcal{E}_0(r,z)=u(r)e^{i\bar{k}z}$. The steady state value for the plasma density will be

$$\rho_0(r) = \sqrt{\frac{b}{a}}|u(r)|^K. \tag{13}$$

Let us investigate a time-perturbed solution consisting of

$$\mathcal{E}(r,z,t) = \mathcal{E}_0(r,z) + \mathcal{E}_+(r,z)e^{-i\Omega t} + \mathcal{E}_-(r,z)e^{i\Omega t}, \tag{14}$$

$$\rho(r,z,t) = \rho_0(r) + \rho_+(r,z)e^{-i\Omega t} + \rho_+^*(r,z)e^{i\Omega t}, \tag{15}$$

where $\mathcal{E}_+$, $\mathcal{E}_-$, and ρ_+ are small compared to $\mathcal{E}$ and ρ, respectively.

First, we solve the plasma equation to find $\rho_+(r,z)$, by inserting the perturbed solution for ρ, and keeping only terms linear in the perturbations. Equating terms that oscillate as $e^{-i\Omega t}$ gives

$$\rho_+ = \frac{Kb|\mathcal{E}_0|^{2K-2}(\mathcal{E}_0^*\mathcal{E}_+ + \mathcal{E}_0\mathcal{E}_-^*)}{2a\rho_0 - i\Omega}. \tag{16}$$

With the terms oscillating as $e^{i\Omega t}$, we obtain the complex conjugate of this equation. Next, we take this solution for ρ_+ and the full form for $\mathcal{E}$, insert them into the propagation equation (1), and expand terms, keeping only linear perturbation terms. The zero order terms $\mathcal{E}_0$ and ρ_0 satisfy Eq. (1) without the loss terms. For the first-order terms oscillating as $e^{\mp i\Omega t}$, we obtain

$$\frac{\partial \mathcal{E}_\pm}{\partial z} = \frac{i}{2k}\nabla_\perp^2\mathcal{E}_\pm + ik_0n_2[2|\mathcal{E}_0|^2\mathcal{E}_\pm + \mathcal{E}_0^2\mathcal{E}_\mp^*] - i\frac{\sigma\omega\tau}{2}\left(\rho_0\mathcal{E}_\pm + \frac{Kb|\mathcal{E}_0|^{2K-2}}{2a\rho_0 - i\Omega}[|\mathcal{E}_0|^2\mathcal{E}_\pm + \mathcal{E}_0^2\mathcal{E}_\mp^*]\right). \tag{17}$$

These two equations give the evolution of the coupled perturbation fields $\mathcal{E}_+$ and $\mathcal{E}_-$.

We can analytically treat the case for which the steady state solution is a plane wave. Let the perturbation fields also be plane waves, defined as follows:

$$\mathcal{E}_+(r,z) = u_+\exp(\lambda z + i\bar{k}z + i\mathbf{k}_\perp\cdot\mathbf{r})$$

$$\mathcal{E}_-(r,z) = u_-\exp(\lambda^* z + i\bar{k}z - i\mathbf{k}_\perp\cdot\mathbf{r}), \tag{18}$$

where $\mathbf{k}_\perp$ is the transverse wave vector and $\mathbf{r}$ is the transverse coordinate. When we insert these forms into the above equations for $\mathcal{E}_+$ and $\mathcal{E}_-$ and cancel the exponential dependence, we find

$$(i\bar{k} + i\bar{k}_\perp + \lambda)u_+ = iB[2u_+ + u_-^*] - iC(\rho_0 u_+ + A(\Omega)[u_+ + u_-^*]), \tag{19}$$

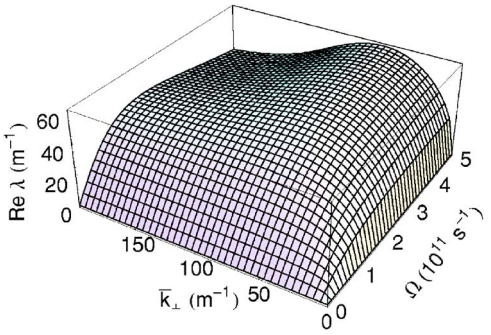

FIG. 6. Growth rate vs $\bar{k}_\perp$ and Ω, for intensity 3.2×10^{16} W/m^2.

$$(i\bar{k} + i\bar{k}_\perp + \lambda^*)u_- = iB[2u_- + u_+^*] - iC(\rho_0 u_- + A^*(\Omega)[u_- + u_+^*]), \tag{20}$$

where

$$A(\Omega) \equiv \frac{Kb|\mathcal{E}_0|^{2K}}{2a\rho_0 - i\Omega}, \quad B \equiv k_0n_2|\mathcal{E}_0|^2, \quad C \equiv \frac{\sigma\omega\tau}{2}, \tag{21}$$

and $\bar{k}_\perp \equiv k_\perp^2/2k$. Eq. (19), combined with the complex conjugate of Eq. (20), gives a matrix equation

$$M\begin{bmatrix} u_+ \\ u_-^* \end{bmatrix} = \begin{bmatrix} i(\bar{k}+\bar{k}_\perp) + \lambda & \\ & -i(\bar{k}+\bar{k}_\perp) + \lambda \end{bmatrix}\begin{bmatrix} u_+ \\ u_-^* \end{bmatrix}, \tag{22}$$

where

$$M = i\begin{bmatrix} 2B - C(\rho_0 + A) & B - AC \\ AC - B & C(\rho_0 + A) - 2B \end{bmatrix}. \tag{23}$$

A nontrivial solution to this only exists if

$$\lambda^2 = Y^2 - (X - \bar{k} - \bar{k}_\perp)^2, \tag{24}$$

where we define $X \equiv 2B - C(\rho_0 + A)$ and $Y \equiv B - AC$. The above result for λ^2 factors as

$$\lambda^2 = -(B - C\rho_0 - \bar{k} - \bar{k}_\perp)[3B - C(\rho_0 + 2A) - \bar{k} - \bar{k}_\perp]. \tag{25}$$

The propagation constant $\bar{k}$ for a plane wave solution with amplitude $\mathcal{E}_0$ is $k_0\overline{\Delta n}$ where $\overline{\Delta n}$ is the induced nonlinear refractive index. In this case $k_0\overline{\Delta n} = k_0n_2|\mathcal{E}_0|^2 + k_0n_3|\mathcal{E}_0|^3$. From the definitions of B and C, and the steady state value n_3, this is also equal to $B - C\rho_0$ for a plane wave solution. Thus we can write

$$\lambda^2 = \bar{k}_\perp[2(B - AC) - \bar{k}_\perp] = 2Y(\Omega)\bar{k}_\perp - \bar{k}_\perp^2. \tag{26}$$

This implies positive and negative roots, and thus unstable growth, for all frequencies Ω, except where $\lambda = 0$.

Figure 6 shows an example of the growth rate Re(λ) plotted against $\bar{k}_\perp$ and Ω. The growth rate is everywhere positive, except for $\bar{k}_\perp = 0$ or $\Omega = 0$, since we must choose the positive root of λ^2. We expect zero growth for $\bar{k}_\perp = 0$, since

this corresponds to a uniform plane wave intensity correction. Additionally, we have chosen an intensity large enough such that the plane wave solution is stable for $\Omega=0$. The form of this growth rate is similar to that obtained by Couairon and Bergé [52] and Bian *et al.* [57] for comparable propagation equations.

For large values of $\bar{k}_\perp$, a Taylor series approximation shows that the value of $\mathrm{Re}(\lambda)$ approaches $-\mathrm{Im}(Y)$. For larger values of Ω, there will be a $\bar{k}_\perp$ corresponding to peak growth rate. For small values of Ω, the peak growth rate is an asymptotic value as $\bar{k}\to\infty$. There is no cutoff in the growth rate for large values of $\bar{k}_\perp$; however, the value of $\bar{k}_\perp$ is effectively limited by its relationship to $k_\perp$, the transverse wave vector, which is assumed to be small compared to k_z in the paraxial approximation.

For $\Omega=0$, a growing mode corresponds to a purely spatial modulational instability. For plane wave solutions, the stability of the solution depends on the intensity $|\mathcal{E}_0|^2$. In this case

$$\lambda^2 = 2[Y(\Omega=0)]\bar{k}_\perp - \bar{k}_\perp^2, \tag{27}$$

where $Y(\Omega=0)=B-A(\Omega=0)C$ can be shown to be equal to

$$k_0 n_2|\mathcal{E}_0|^2 + (3/2)k_0 n_3|\mathcal{E}_0|^3. \tag{28}$$

If $n_2+(3/2)n_3|\mathcal{E}_0|>0$, then $Y(0)$ is positive, and there will be unstable modes for certain values of $\bar{k}_\perp$. Above the cutoff intensity, the plane wave solution is stable with respect to purely spatial modulations. For the UV filament example in this paper, this cutoff intensity is given by $|\mathcal{E}_0|^2\approx 2.4\times 10^{16}$ W/m^2.

As $\Omega\to\infty$, the instability growth rate does not die off, nor is there an upper cutoff, as in some cases for modulational instability that only consider self-focusing and GVD [50,51]. Instead, λ^2 approaches the limit $\bar{k}_\perp(2B-\bar{k}_\perp)$. For values of $\bar{k}_\perp$ within the unstable range $0<\bar{k}_\perp<2B$, the solutions are unstable even as $\Omega\to\infty$. For the 3.2×10^{16} W/m^2 solution used to generate the previous figure for the eigenvalues, the value of $2B$ is 126 m^{-1}. This can be explained by examining what happens to the equations in the stability analysis. If we take $\Omega\to\infty$, we remove all the effects of the stabilizing n_3 or plasma term from the coupled equations, and since there are no dissipation terms present, we are left with the stability of the Kerr medium, which is known to be spatially unstable [37,38,53].

We examine the stability of UV filaments in three ways. First, the plane wave stability model predicts the growth rate as a function of a single transverse wave vector $\mathbf{k}_\perp$ and temporal perturbation frequency Ω. This analysis predicts unstable growth for all frequencies Ω. Next, given a single temporal frequency Ω and a steady state solution $\mathcal{E}_0$, we can solve the equations for the coupled perturbation fields, given by Eq. (17). This gives results for all transverse wave vectors $\mathbf{k}_\perp$ that are represented by the numerical grid. Finally, we model the full three-dimensional propagation, by including the time dimension of a pulse as the third transverse dimension in the split-operator propagation. This will allow observation of unstable growth for all frequencies Ω and $\mathbf{k}_\perp$ that we can numerically represent.

IV. GROWTH OF UNSTABLE MODES

A. Coupled perturbation fields

We first examine the results for the propagation of the coupled perturbation fields $\mathcal{E}_+$ and $\mathcal{E}_-$ described in the linear stability analysis. This propagation is performed using a split-step method with two fields; the coupling is represented by a matrix, which is not Hermitian, since it allows for growth of the fields. This forbids a unitary transformation approach for propagation; instead, the matrix exponential is directly computed. The results tell us about the shape and growth rate of the perturbation fields, but they are based on a linear approximation, and only model the growth for one temporal frequency Ω at a time.

The steady state field $\mathcal{E}_0$ is an input to this model. It can be chosen to be either a computed beam solution, or a plane wave. The choice of a plane wave was used to verify the code with respect to the plane wave growth rate results. The perturbation fields are seeded with either a single plane wave frequency or a uniform complex noise field. Since the stability analysis is linear, there is no dependence on amplitude, and the mode will grow without bound as the coupled fields evolve. However, this approach provides a tool to isolate the shape of the most unstable mode, as this mode will grow fastest, and eventually dominate, as the fields propagate.

With a steady state beam solution $\mathcal{E}_0$, we find unstable growth for all frequencies $\Omega>0$, as predicted. The growth rates do not exactly correspond to the plane wave prediction, because the $\mathcal{E}_0$ beam solution contains a combination of plane waves with differing $\bar{k}_\perp$ values. The intensities of these plane wave components are lower than the peak intensity of the beam solution; lower intensities tend to result in lower growth rates. We have investigated the growth of unstable modes for several frequencies Ω; we discuss the results here for the example cases of $\Omega=0, 10^{11}$, and 10^{12} s^{-1}. We use the steady state solution $\mathcal{E}_0$ computed in Sec. II D with a peak intensity of 3.2×10^{16} W/m^2.

For $\Omega=0$, one might not expect any instability growth, since we chose the peak intensity of the steady state solution to be above the stability cutoff. However, an unstable mode still grows for $\Omega=0$, no matter how carefully we choose the steady state solution or adjust the grid size or resolution. The unstable mode is circularly symmetric, with a growth rate λ on the order of 10^{-2} m^{-1}. The explanation for this unstable growth is that the solution for $\mathcal{E}_0$ is composed of plane waves that can have a lower intensity than the cutoff for unstable growth under purely spatial instability. Thus a small portion of the field seeds growth at $\Omega=0$.

Figure 7(a) shows the form of the real part of the perturbation field $\mathcal{E}_+$ for $\Omega=10^{11}$ s^{-1}. The field $\mathcal{E}_-$ is related to the complex conjugate of $\mathcal{E}_+$ and is not shown. The fields take the form of two lobes; when they initially develop, the two lobes may not have the same height. However, as this strongest mode grows, the two lobes become equal in height. The early asymmetry is due to the presence of other, slower growing modes, seeded by the initial noise. However, the shape of the fastest growing mode eventually dominates. Since the propagation equations have azimuthal symmetry, the choice of orientation of the two lobes is determined by

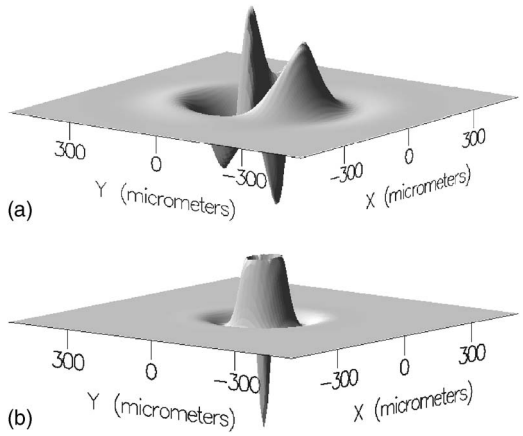

FIG. 7. Coupled perturbation field shape (arbitrary units) $\mathcal{E}_+$ for $\Omega=10^{11}$ and 10^{12} s^{-1}.

the initial noise seed. The strongest growth rate for $\Omega=10^{11}$ s^{-1} is approximately 13 m^{-1}, which, as seen from Fig. 6 is lower than the general neighborhood of linear growth rates, given this value of Ω. The peak plane wave growth rate for $\Omega=10^{11}$ s^{-1} is roughly 35 m^{-1}.

Figure 7(b) shows the form of the real part of the perturbation field $\mathcal{E}_+$ for the case of $\Omega=10^{12}$ s^{-1}. For this frequency, the growing field initially appeared to have the two-lobe structure that was observed for $\Omega=10^{11}$ s^{-1}. However, as the field is propagated, the structure becomes symmetrical. Thus for $\Omega=10^{12}$ s^{-1}, the growth rate for the symmetric mode is higher than the rate for the asymmetric modes. This growth rate is approximately 40 m^{-1}, while the peak plane wave growth rate for this frequency is roughly 60 m^{-1}. As the perturbation evolves, the absolute value approaches a fixed shape, but the real and imaginary parts continuously exchange form. This makes the beam become lopsided, and oscillate in the manner of a "snake" or "neck" instability, depending on whether the mode is asymmetric or symmetric [53].

B. Periodic boundary conditions in time

We now turn to the case in which the solution is fully resolved in the time domain, and we use a three-dimensional propagation code. We first consider periodic boundary conditions in time. This allows investigation of the stability of a CW beam, or the central region of a hypothetical long pulse. We initialize the temporal profile as flat, but with some small random noise.

Recall that the stability analysis indicates that unstable modes are expected to grow for all temporal frequencies. Thus, if the noise seed contains all available frequency components, the noise will grow for all frequencies allowable on the grid. If the noise is spectrally limited to lower frequency components, the spectrum of the growing noise will be approximately cut off at this limit; however, higher frequency components eventually appear, due to the coupling between space and time in the plasma response.

As a diagnostic example, we initialize the field with the steady state solution for $\mathcal{E}_0$ shown in Fig. 5, with peak intensity 3.2×10^{16} W/m^2. The noise is 1 percent random amplitude variation over the full 3D grid, bandwidth limited to $|\Omega|<10^{12}$ s^{-1} and $k_\perp<2\times10^5$ m^{-1}. The results of the propagation for three different distances are shown in Fig. 8. The figures show plots of the absolute value of the field amplitude taken in cross section, for the central ($y=0$) two-dimensional slice of the full three-dimensional field. The ini-

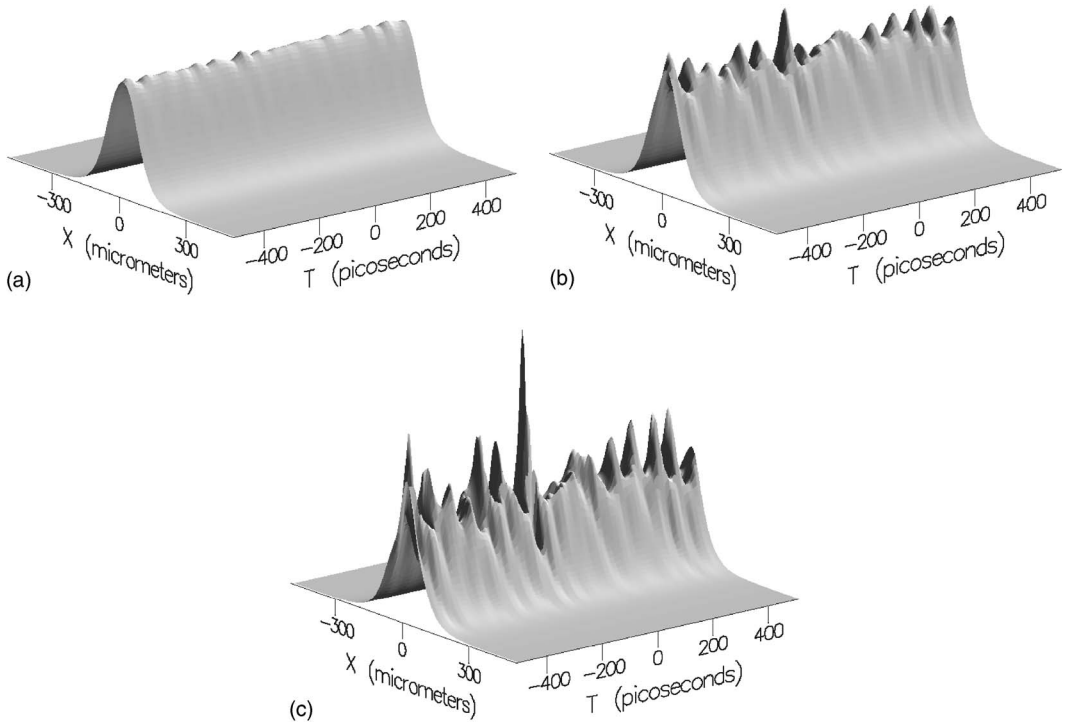

FIG. 8. Growth of instability for periodic boundary conditions in time.

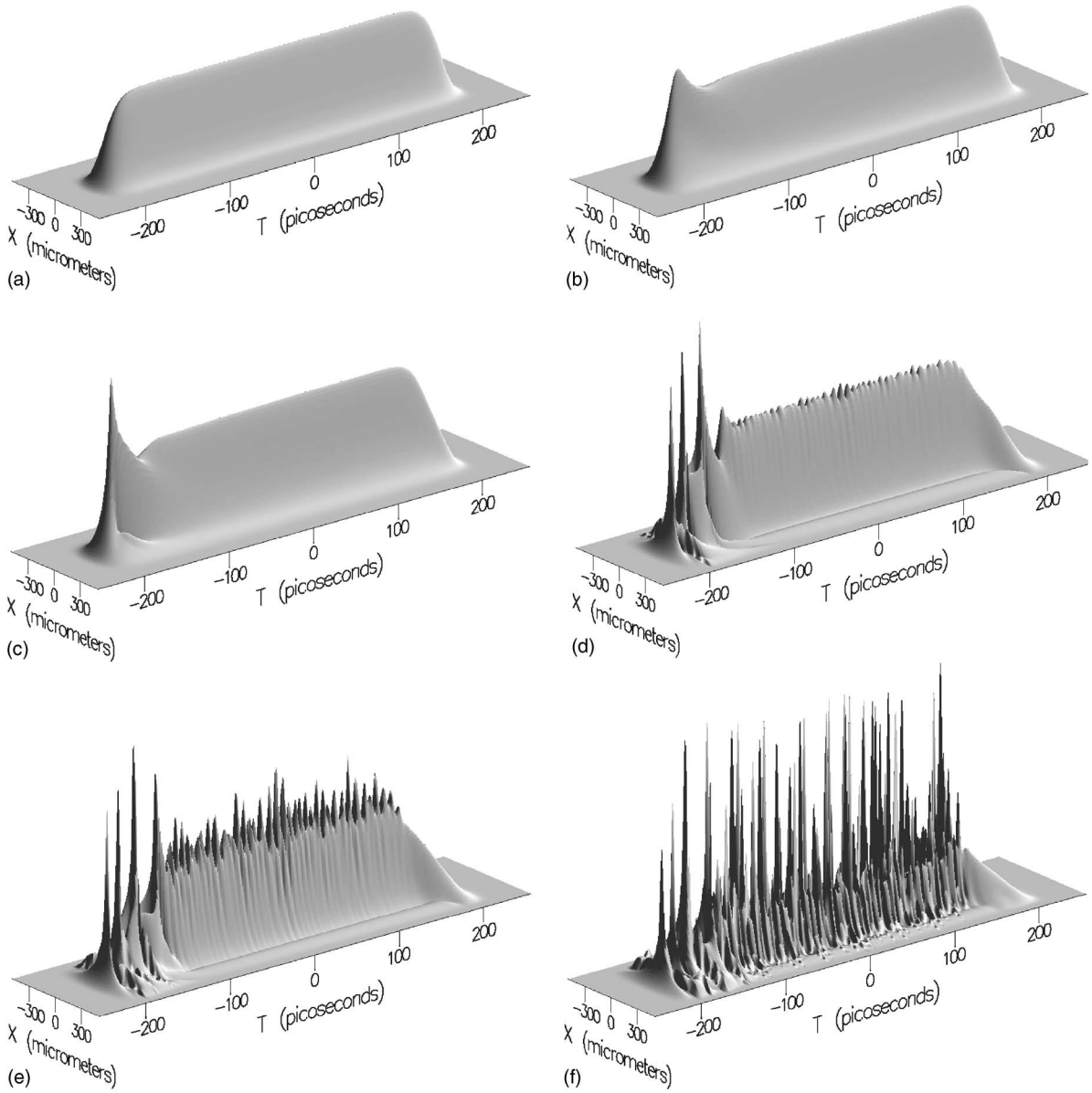

FIG. 9. Amplitude of a finite duration pulse with noise seed and absorption.

tial condition is not shown, as the amplitude of the noise is initially too small to see. Both symmetric and antisymmetric (neck and snake) modulations are observed [53].

As the field evolves, the instability grows until it becomes so strong that it exceeds the numerical resolution of the grid; the time or length scales of the features of the noise peaks can approach the grid spacing in space or time. However, this analysis provides a useful look at the initial growth of a modulational instability. For the UV filaments studied here, it is apparent from these results that the steady state solution suffers from the instability and will fragment. Thus, for a pulse with finite duration, we expect that the transient leading edge of the pulse will not be able to converge to the steady state solution that represents the central flat temporal region of the pulse. We model such a pulse in the next section.

V. PULSE PROPAGATION

A. 3D propagation

To simulate a finite duration pulse, we prepare the field with a temporal pulse profile that resolves the edges of the pulse, and we remove the periodic boundary conditions in time. The initial temporal profile is chosen as a super-Gaussian, defined as follows:

$$\mathcal{E}(t) \propto \exp\{-[(t-t_0)^2/t_p^2]^M\}, \tag{29}$$

where M is the super-Gaussian order. This allows examination of a pulse that contains both transient effects at the edges and a central flat region. We initialize the spatial profile to match the exact computed stationary solution, for diagnostics, or to a Gaussian beam profile, to represent what might be experimentally generated.

The initial condition was a spatial Gaussian defined with peak power exactly 500 MW, and width 120 μm. These values were chosen so that the peak intensity was greater than the plane wave cutoff for stability in the $\Omega=0$ analysis, but the specific power was otherwise arbitrary. The instability and pulse consumption to be presented below are examples of the effects which occur for any power level that supports a self-trapped beam.

The temporal super-Gaussian was of order $M=10$, with $t_p=200$ ps, giving a pulse of roughly 400 ps in duration. The noise seed was 0.01 percent random amplitude variations, bandwidth limited to $|\Omega|<10^{12}$ s^{-1}. Figure 9 shows the propagation of the pulse. As the pulse propagates, it develops a series of collapse events on the leading edge. These collapses are seeded by the transient shape of the edge, which does not match a steady solution. During each collapse, the intense plasma causes the field to dip in amplitude and temporarily form a ring, which then seeds the next collapse. These self-focusing collapse events appear to consume the pulse at a roughly linear rate; for the power in the example, this rate is roughly 200 ps/m. The trailing edge independently breaks apart into a ring, but does not cause any collapse events.

The consumption of the pulse by collapse, while it arises from the transient behavior at the beginning of the pulse, does not appear to be itself a transient effect. That is, it does not decay; it maintains a steady rate of consumption of the pulse. The noise growth destroys the pulse globally, as opposed to the collapse events, which consume the pulse from the leading edge to the trailing edge.

Fully resolving the collapsed peaks requires modeling arrest mechanisms such as GVD, using time resolution on the order of femtoseconds. However, in our simulations, the peaks tend to collapse to dimensions comparable to the grid spacing in time; in the example shown, the propagation results are numerically contaminated by Fig. 9(f). There are numerical dispersion effects induced by the finite spectral bandwidth of the grid that act to limit the collapse [37]. The simulation has been done with multiple values of Δt to check the convergence, and in all cases the general structure of the overall result is consistent with respect to the qualitative features, such as the spacing of the peaks and the consumption rate. An example of this comparison is shown for the on-axis amplitude at $z=25$ cm in Fig. 10.

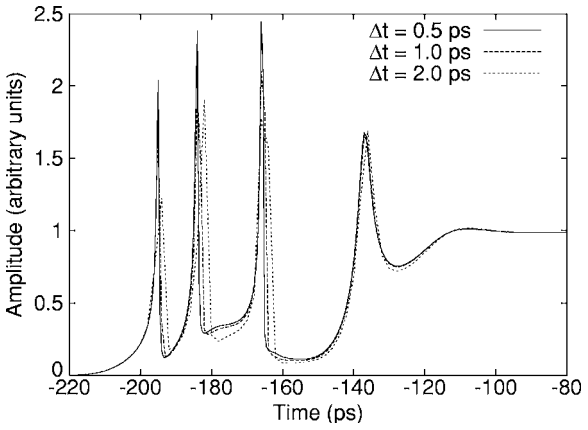

FIG. 10. Comparison of collapse events for multiple values of Δt. The plot shows the on-axis amplitude of the field at $z=25$ cm during the initial portion of the pulse, for three different values of Δt.

B. Fluence behavior

To determine the combined effect of the linear consumption and the exponential growth of the instability, we can examine the fluence, and its width, computed with a second-moment method. Figure 11 shows the fluence profiles corresponding to the simulation in the previous section of the 470 MW peak power pulse propagated with noise and loss present in the model. The impact of the pulse collapse on the fluence depends on the fraction of the pulse's temporal width that has collapsed. For this example, at roughly 30 cm, the noise has begun to dominate, which begins to significantly affect the fluence profile. Up to that point, the fluence profile is not significantly affected by the collapsing front edge.

Figure 12 shows the width of the fluence profile as a function of propagation distance for the finite duration pulse. The fluence profile width initially decreases, since the initial condition was chosen to have a spatial width larger than the corresponding stationary solution. This is in agreement with the oscillations predicted by the Schwarz-Diels model. Then, the pulse stays confined, until about 30 cm. During this phase, the leading edge of the pulse is consumed by transient collapse. The effect that this has on the width of the total fluence is dependent on the duration of the pulse; for a longer initial pulse, a given consumption rate in ps/m affects a smaller fraction of the pulse, and has less of an impact on the fluence profile. However, once the exponentially growing instability becomes significant, in this case around 30 cm, it quickly spreads the beam width. Since the noise is seeded uniformly along the pulse, the instability acts as a global effect, and its exponential growth quickly dominates until it saturates.

If one is only interested in the fluence at the target, the claim could be made that the pulse propagates successfully up to the point where the noise growth dominates. This point is determined by the initial amplitude of the noise and the growth rate of the noise, which is is roughly 10–20 cm^{-1}, corresponding to a growth length of 5–10 cm. For this example, the fluence profile width stays confined until about 40 cm, somewhat more than the Rayleigh range on the order of 10 cm. A pulse could be prepared to propagate farther in a steady confined fashion if the intensities were lower and the initial noise was controlled, but not for distances on the order of kilometers. However, the analysis does not rule out the possibility of the propagation of some complicated dynamic mode involving multiple filaments over longer distances.

C. Length scales

The fundamental length scale for a Gaussian beam is the Rayleigh range $\pi w_0^2/\lambda$, where w_0 is the beam waist radius. "Long distance propagation" is considered relative to this scale. For the example beams that we have considered, the waist size w_0 is on the order of 100 μm. In the ultraviolet at

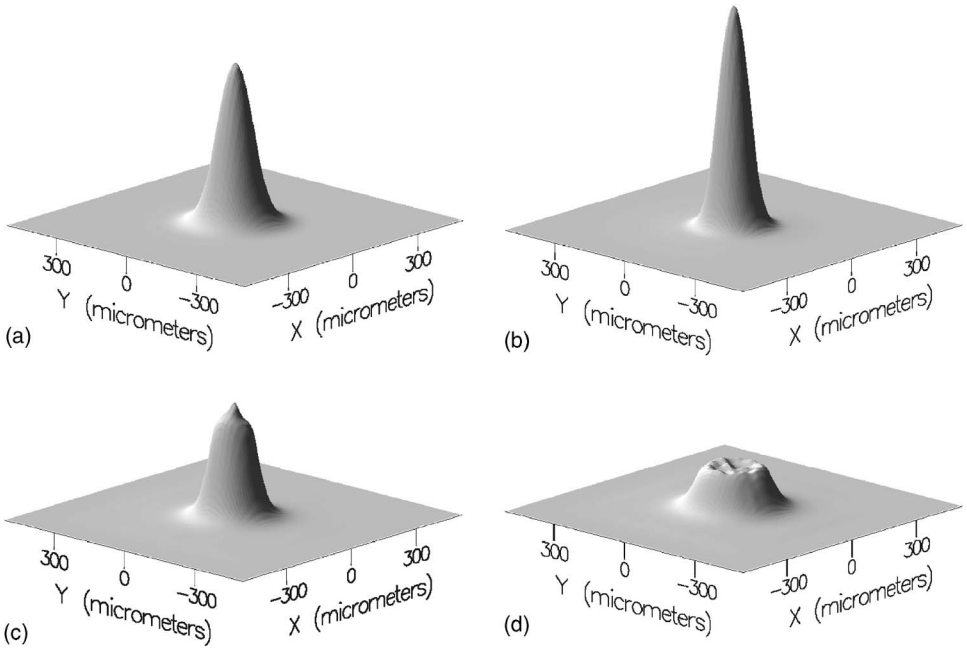

FIG. 11. Fluence profiles for the finite duration pulse, at several propagation distances.

248 nm, this gives a Rayleigh range on the order of 10 cm.

The length scale for linear (Rayleigh scattering) loss is given by $1/\alpha_l \approx 2$ km in the ultraviolet at 248 nm [26]. This is the power $1/e$ length for linear loss. The nonlinear absorption depends on the field intensity and thus the power in the beam. Given the power loss, a rough estimate for the nonlinear absorption $1/e$ length for power is 20 m.

The modulational instability growth rate is on the order of 10–20 m^{-1}, making the growth length scale roughly 5–10 cm. These growth rates become smaller as beam power decreases. For the power in the example, the transient collapse consumption rate was 200 ps/m. This means that, neglecting instabilities, for a pulse on the order of 1 ns, the propagation distance before complete consumption and collapse is roughly 5 m.

Table II summarizes some of the pertinent length scales for ultraviolet propagation. The instability growth scale is comparable to the Rayleigh range. The absorption, both linear and nonlinear, is not strong enough to counter the instability before it fragments the pulse. However, to study the behavior and find the distance at which the instability saturates, one needs to evaluate the nonlinear absorption at the intensity of the local collapse peaks.

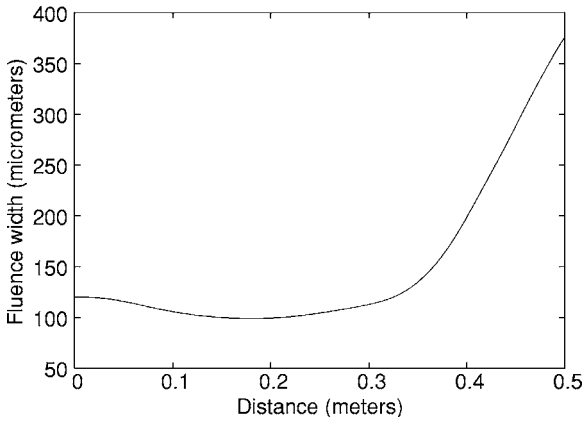

FIG. 12. Width of fluence profile for the realistic pulse. The initial decrease in width is characteristic of the oscillations predicted by the Schwarz-Diels model. This pulse travels roughly four Rayleigh ranges before being destroyed by the modulational instability.

VI. IMPLICATIONS

A. Experimental

Given the numerical results, we expect that the instability and transient consumption of the pulse will have a significant effect on the propagation of ultraviolet filaments. For our example case, a UV filament of duration on the order of a nanosecond may propagate for distances on the order of meters before it is consumed by collapse events. As discussed in the previous section, this still may be described as long distance propagation, for many Rayleigh ranges, given the spatial width of the filament. However, the results do not support hopes of kilometer scale atmospheric propagation of a stable pulse described by a time-independent model in the

TABLE II. Typical length scales for 470 MW peak power UV filaments.

Name	Value	Units
Rayleigh range	10	cm
Linear loss length	2000	m
Nonlinear absorption length	≈20	m
Instability growth length	≈5–10	cm
Pulse consumption distance	t_p/(200 ps/m)	m
Raman scattering	0.01–10	m
Upper limit (avalanche ionization)	≈4–60	ns
Lower limit (plasma rise time)	≈30–200	ps

ultraviolet; the proposal that UV pulse results can scale to longer durations is not supported. For the purpose of energy delivery, one may not be concerned with fragmentation of the pulse in the time direction, as long as the fluence profile is confined. However, the modulational instability also increases the width of the fluence profile (Fig. 12). The rate at which the modulational instability fragments the main body of the pulse is faster than the transient consumption. The point at which this fragmentation occurs depends on how much noise is initially present, but due to the exponential growth rate, the onset of this instability cannot be significantly postponed.

B. Theoretical

A steady state or long pulse model may simplify theoretical predictions, but if the physics of the problem admit the effects of modulational instability combined with other transient effects, it is dangerous to apply such a model. The presence of such effects, which we have demonstrated for the case of UV filament propagation, violates the basic steady state beam assumption that is used in the long pulse model.

We have shown that long duration (nanosecond scale) UV filaments suffer from these effects, limiting their effective propagation range as described by a steady state theory to meters. This prevents the short-duration results from scaling to longer UV pulses in the form of a steady beam as desired [25,27]. In the case of UV filaments, the time-independent method is an oversimplification of the dynamics of long pulse propagation.

In general, caution must be used when describing solutions of reduced 2D time-independent versions of full 3D equations. For example, the treatment by Skarka *et al.* of vortex solitons [28] relies on considering the evolution of a single time slice of a pulse, which simplifies the propagation to a time-independent form [15]. This allows the use of a variational technique to describe the spatial form of the vortices. They emphasize the spatial stability of the vortex solutions, but do not consider the full temporal dynamics or stability of the pulse. This time-independent method limits the applicability of the claim that such solitons will be able to propagate for appreciable distances in air, until a full temporal analysis is performed.

Additionally, the time-integrated approach of Bergé *et al.* to multiple filamentation [29] results in a similar time-independent propagation equation that admits soliton solutions, but these cannot describe effects such as dynamic replenishment [5,32] and the collapses in both space and time. The dynamic nature of the problem may mean that "long-range" filaments qualitatively describe the results, but the most convincing theory must consider the stability in the time domain.

VII. CONCLUSION

We have considered the propagation of long filaments in air, primarily in the ultraviolet. It had been speculated that previous successful demonstrations of ultraviolet filaments would scale to longer pulse durations [25,27], allowing the propagation of long filaments and delivery of higher energies over long distances through the atmosphere. However, the existing theoretical model for long ultraviolet filaments did not address their stability, or how they are created [27].

To address these issues, we have considered and extended a long pulse model for ultraviolet filaments [27]. We have shown that while it is valid for the domain of pulse durations that it claims, the pulse instability and transient effects cannot be neglected. We investigated the question of stability using three levels of approximation: the plane wave stability results, the evolution of the linearized coupled perturbation fields, and the simulation of full 3D pulses using a time-dependent plasma model. The results were consistent on all three levels, and showed that the modulational instability ultimately results in the fragmentation of the pulse. We also demonstrated that the transient shape of the front edge of the pulse induces a series of collapse events, which also tend to consume a long pulse.

In the case of ultraviolet filaments, we still predict that propagation over several Rayleigh ranges can be achieved, depending on conditions. The transient collapse consumes on the order of hundreds of picoseconds of the pulse per meter of propagation, but keeps the fluence profile relatively confined. The modulational instability, however, destroys the entire pulse as it grows, with a gain length on the order of tens of centimeters, depending on how it is seeded. The values of these consumption rates depend on the model parameters in Table I, which are not accurately known, but the above detrimental effects will still be present even for alternate values. The propagation of long stable pulses described by a steady state model over kilometer-scale distances does not appear feasible, given the effects we have considered. The long pulse model and other methods that eliminate the time dimension have limited prediction power when temporal stability effects are not considered. A steady state model is not suitable for the description of a highly fragmented pulse.

ACKNOWLEDGMENTS

This work is sponsored by the U.S. Air Force Office of Scientific Research (AFOSR), under Grant Nos. AFOSR-F49620-00-1-0312 and AFOSR-F49620-03-1-0194. The views expressed in this article are those of the authors and do not reflect the official policy or position of the United States Air Force, Department of Defense, or the U.S. Government.

[1] R. W. Boyd, *Nonlinear Optics* (Academic Press, New York, 1992).
[2] A. Couairon and L. Bergé, Phys. Rev. Lett. **88**, 135003 (2002).
[3] J. Moloney, M. Kolesik, M. Mlejnek, and E. Wright, Chaos **10**, 559 (2000).
[4] S. Tzortzakis, B. Lamouroux, A. Chiron, M. Franco, B. Prade, and A. Mysyrowicz, Opt. Lett. **25**, 1270 (2000).
[5] M. Mlejnek, M. Kolesik, J. V. Moloney, and E. M. Wright, Phys. Rev. Lett. **83**, 2938 (1999).
[6] F. Courvoisier, V. Boutou, J. Kasparian, E. Salmon, G. Méjean, J. Yu, and J. Wolfe, Appl. Phys. Lett. **83**, 213 (2003).
[7] N. Aközbek, M. Scalora, C. Bowden, and S. Chin, Opt. Commun. **191**, 353 (2001).
[8] J. Kasparian *et al.*, Opt. Lett. **25**, 1397 (2000).
[9] J. Yu, D. Mondelain, G. Ange, R. Volk, S. Niedermeier, and J. Wolf, Opt. Lett. **26**, 533 (2001).
[10] P. Rairoux *et al.*, Appl. Phys. B **71**, 573 (2000).
[11] H. Wille, M. Rodriguez, J. Kasparian, D. Mondelain, J. Yu, A. Mysyrowicz, R. Sauerbrey, J. Wolf, and L. Wöste, Eur. Phys. J. A **20**, 183 (2002).
[12] J.-C. Diels, R. Bernstein, K. E. Stahlkoph, and X. M. Zhao, Sci. Am. **277**, 50 (1997).
[13] X. M. Zhao, J.-C. Diels, C. Y. Wang, and J. M. Elizondo, IEEE J. Quantum Electron. **31**, 599 (1995).
[14] M. Rodriguez *et al.*, Phys. Rev. E **69**, 036607 (2004).
[15] B. La Fontaine, F. Vidal, Z. Jiang, C. Chien, D. Comtois, A. Desparois, T. Johnston, J.-C. Kieffer, and H. Pépin, Phys. Plasmas **6**, 1615 (1999).
[16] G. Méchain, A. Couairon, Y.-B. André, C. D'Amico, M. Franco, B. Prade, S. Tzortzakis, A. Mysyrowicz, and R. Sauerbrey, Appl. Phys. B **79**, 379 (2004).
[17] Y. Shen, Prog. Quantum Electron. **4**, 1 (1975).
[18] S. Tzortzakis, L. Sudrie, M. Franco, B. Prade, A. Mysyrowicz, A. Couairon, and L. Bergé, Phys. Rev. Lett. **87**, 213902 (2001).
[19] A. Braun, G. Korn, X. Liu, D. Du, J. Squier, and G. Mourou, Opt. Lett. **20**, 73 (1995).
[20] A. Campillo, S. Shapiro, and B. Suydam, Appl. Phys. Lett. **23**, 628 (1973).
[21] S. Petit, A. Talebpour, A. Proulx, and S. Chin, Opt. Commun. **175**, 323 (2000).
[22] O. Kosareva, V. Kandidov, A. Brodeur, C. Chien, and S. Chin, Opt. Lett. **22**, 1332 (1997).
[23] E. Nibbering, P. Curley, G. Grillon, B. Prade, M. Franco, F. Salin, and A. Mysyrowicz, Opt. Lett. **21**, 62 (1996).
[24] S. Chin, N. Aközbek, A. Proulx, S. Petit, and C. Bowden, Opt. Commun. **188**, 181 (2001).
[25] J. Schwarz, P. Rambo, J. Diels, M. Kolesik, E. M. Wright, and J. V. Moloney, Opt. Commun. **180**, 383 (2000).
[26] J. Schwarz, Ph.D. thesis, Friedrich-Schiller-Universität, Jena, 2003.
[27] J. Schwarz and J.-C. Diels, Phys. Rev. A **65**, 013806 (2001).
[28] V. Skarka, N. Aleksić, and V. Berezhiani, Phys. Lett. A **319**, 317 (2003).
[29] L. Bergé *et al.*, Phys. Rev. Lett. **92**, 225002 (2004).
[30] N. Aközbek, C. M. Bowden, A. Talebpour, and S. L. Chin, Phys. Rev. E **61**, 4540 (2000).
[31] E. M. Wright, B. L. Lawrence, W. Torruellas, and G. Stegeman, Opt. Lett. **20**, 2481 (1995).
[32] M. Mlejnek, E. Wright, and J. Moloney, Opt. Lett. **23**, 382 (1998).
[33] D. Subbarao, K. Batra, and R. Uma, Phys. Rev. E **68**, 066403 (2003).
[34] D. Subbarao, R. Uma, and H. Singh, Phys. Plasmas **5**, 3440 (1998).
[35] V. Magni, G. Cerullo, and S. De Silvestri, Opt. Commun. **96**, 348 (1993).
[36] G. Cerullo, A. Dienes, and V. Magni, Opt. Lett. **21**, 65 (1996).
[37] J. Marburger, Prog. Quantum Electron. **4**, 35 (1975).
[38] S. C. Cerda, Ph.D. thesis, Imperial College of Science, Technology and Medicine, University of London, 1994.
[39] D. Anderson, Phys. Rev. A **27**, 3135 (1983).
[40] G. Fibich and A. L. Gaeta, Opt. Lett. **25**, 335 (2000).
[41] G. Fibich and G. Papanicolaou, SIAM J. Appl. Math. **60**, 183 (1999).
[42] D. Anderson and M. Bonnedal, Phys. Fluids **22**, 105 (1979).
[43] L. Thylén, Opt. Quantum Electron. **15**, 433 (1983).
[44] J. Schwarz, P. Rambo, and J. Diels, Appl. Phys. B **72**, 343 (2001).
[45] A. Couairon, Phys. Rev. A **68**, 015801 (2003).
[46] J. M. Soto-Crespo, D. R. Heatley, E. M. Wright, and N. N. Akhmediev, Phys. Rev. A **44**, 636 (1991).
[47] J. Soto-Crespo, E. Wright, and N. Akhmediev, Phys. Rev. A **45**, 3168 (1992).
[48] R. Chiao, E. Garmire, and C. Townes, Phys. Rev. Lett. **13**, 479 (1964).
[49] K. D. Moll, A. L. Gaeta, and G. Fibich, Phys. Rev. Lett. **90**, 203902 (2003).
[50] G. P. Agrawal, *Nonlinear Fiber Optics* (Academic Press, New York, 1995).
[51] L. W. Liou, X. D. Cao, C. J. McKinstrie, and G. P. Agrawal, Phys. Rev. A **46**, 4202 (1992).
[52] A. Couairon and L. Bergé, Phys. Plasmas **7**, 193 (2000).
[53] V. Zakharov and A. Rubenchik, Sov. Phys. JETP **38**, 494 (1974).
[54] H. C. Yuen and W. E. Ferguson, Jr., Phys. Fluids **21**, 1275 (1978).
[55] T. Lehner and N. Auby, Phys. Rev. E **61**, 1996 (2000).
[56] V. Kandidov, O. Kosareva, and S. Shlenov, Quantum Electron. **27**, 441 (1997).
[57] Z. Bian and T. M. Antonsen, Jr., Phys. Plasmas **8**, 3183 (2001).
[58] A. Campillo, S. Shapiro, and B. Suydam, Appl. Phys. Lett. **24**, 178 (1974).